

# AC Quantum Transport: Formalisms and Applications

Siddhant Midha\*

Department of Electrical Engineering,  
Indian Institute of Technology Bombay  
Powai, Mumbai, India, 400076  
(Dated: May 4, 2023)

With the advent of possible beyond-Moore scaling in today's technology, devices nowadays have become immensely compact, thereby necessitating a clear understanding of the quantum mechanical phenomenon underlying these nanoscale devices. There has been significant progress in the development of time *independent* quantum transport formalisms (DC case), viz., the non-equilibrium Greens' function (NEGF) method and the scattering method to understand the exciting physics which lies at the forefront of current condensed matter research. Now, there is a need for the extension of such formalisms to the time *dependent* regime (the AC case); applications involve many superconducting areas (AC Josephson effect, superconducting quantum bits), excitations in the quantum hall phase, measurement of photo-assisted shot noise etc. In this article, we discuss the extensions of the NEGF and the scattering formalisms in the AC regimes: We review the currently developed theory, elucidate using simple numerical examples, discuss advanced applications made possible owing to these AC quantum transport formalisms.

## I. INTRODUCTION

Much of the impressive technological feats achieved in current days owe a significant portion to the development of techniques – both experimental and simulation – of working with nanoelectronics devices. The tight-binding method is perhaps one of the most common tools used to analyze such systems, and allows for the modelling of various degrees of freedom – spin, lattice, valley etc. – for running state-of-the-art simulations of these devices. Notable examples include graphene devices [1, 2], spintronic devices [3, 4], topological insulators [5–7] and hybrid superconducting-semiconducting systems with applications to topological quantum computing [8, 9].

On the simulation side of things, two methods are prominently used to model these nanoelectronic devices under the tight binding scheme, viz., the non-equilibrium Green's function (NEGF) method [10] and the scattering matrix approach [11]. Prominently, the developments in both these methods until now is for the *time independent* case, wherein the transients are not dealt with, and one studies DC quantities such as the conductance, currents across leads (spin currents and charge currents), electronic density etc. Moreover, these methods are developed enough to simulate exotic phenomenon such as hybrid junctions and topological insulators.

It has recently been found that when mesoscopic systems are probed at non-zero frequencies (i.e., the *time dependent* case), entirely new physics is revealed and insight into the time-scales of the quantum system under consideration is obtained. This has been investigated as effects such as quantum capacitance, finite frequency shot noise, quantum pumping and spin pumping, etc. Experimentally, there has been a lot of work with

manipulating quantum bits, for example using superconducting systems, via microwave pulses (thus, an AC phenomenon). Simulation methodologies for such time-dependent regimes are now under development – both the NEGF method and the scattering approaches are being extended to the time-dependent case. This development is more non-trivial than the DC case. Opposed to the DC case, here the AC response is very sensitive to the distribution of the internal potential in the sample, which is a consequence of the charge distributions (generated by the voltages or currents applied at the contacts) and must be calculated self-consistently [12]. Moreover, there is a characteristic frequency  $\omega_c$ , at which the conductance deviates from the dc value, which in turn depends on the internal timescales of the system. Thus, AC transport is a non-trivial generalization of the DC case, and provides more insight into the system when the probing frequency matches the internal frequencies.

In this brief review paper, we aim to provide a pedagogical and sufficiently technical introduction to the field of AC quantum transport. We start by reviewing the NEGF formalism, and various works which aim to develop AC-NEGF with some simple examples of their numerical implementations in Sec. II. Next, we move on to the scattering formalism and talk about the work done in extending it to the AC case, again with numerical examples in Sec. III. Particularly, we discuss the KWANT [13] and the TKWANT[14] packages, and how they have used the scattering formalism for the DC and AC case respectively. In Sec. IV we use the TKWANT package to (i) review a simple example and illustrate the use of TKWANT, and (ii) perform previously unknown simulations as an attempt to validate the usefulness of AC simulations. We then briefly discuss advanced applications of such AC formalisms by reviewing some hot topics investigated involving AC regimes. Finally, we conclude the paper in Sec. V.

---

\* siddhantm@iitb.ac.in

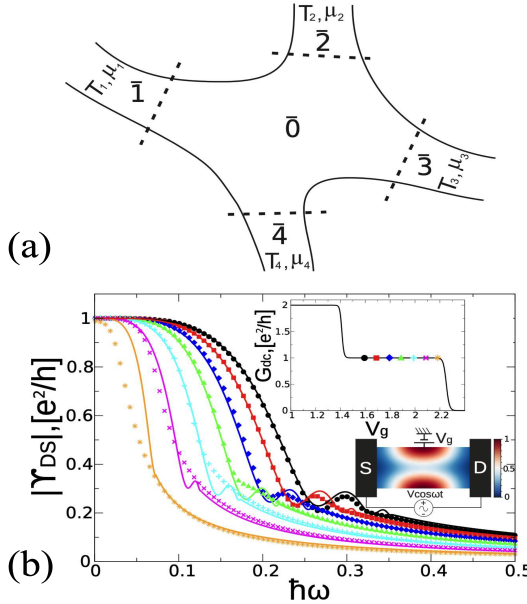


FIG. 1. (a) A typical device schematic studied under the NEGF approach: the  $\bar{0}$  labels the finite scattering region, which is connected to different leads  $\bar{m}$ ,  $m \neq 0$  maintained at temperature  $T_m$  and chemical potential  $\mu_m$  (b) Absolute value of the conductance across a quantum point contact (QPC), simulated using the AC-NEGF method, for different  $V_g$  values depicted on the inset. The inset shows the DC conductance as a function of  $V_g$ . Lower inset shows potential profile formed across the QPC. Figures adapted from [15]

## II. THE NEGF METHOD

### A. Numerical Cookbook using NEGF

Here, we review the work in [15]. We consider a tight-binding hamiltonian of the form

$$\hat{\mathbf{H}} = \sum_{n,m} \mathbf{H}_{nm} c_n^\dagger c_m \quad (1)$$

where  $c_i^\dagger$  ( $c_i$ ) are the creation (annihilation) operators on site  $i$ . With this hamiltonian, the full retarded Green's function is given as,

$$\mathcal{G}(E) = (E + i\eta - \mathbf{H})^{-1} \quad (2)$$

We visualize the system under study as a scattering region  $\bar{0}$  connected to leads labelled by  $\bar{m}$ ,  $m \neq 0$ , see Fig. 1. We integrate out the electrodes to obtain the retarded Green's function inside the device region,

$$\mathcal{G}_{\bar{0}\bar{0}}(E) = (E + i\eta - H - \sum_{m=1} \Sigma^r(m; E))^{-1} \quad (3)$$

where  $H = \mathbf{H}_{\bar{0}\bar{0}}$  is the hamiltonian projected onto the device region, and  $\Sigma^r(m; E)$  is the retarded self-energy due to lead  $m$ , given as,

$$\Sigma^r(m; E) = \mathbf{H}_{\bar{0}\bar{m}}(E + i\eta - \mathbf{H}_{\bar{m}\bar{m}})^{-1} \mathbf{H}_{\bar{m}\bar{0}} \quad (4)$$

Such self-energies can be obtained by recursive techniques [10]. Observables, such as current are given as,

$$I_m = \frac{e}{h} \int dE \sum_{m'=1}^N (f_m - f_{m'}) Tr[\mathcal{G}_0 \Gamma_{m'} \mathcal{G}_0^\dagger \Gamma_m] \quad (5)$$

where  $f_m$  is the fermi function at lead  $m$ , and the broadening matrix  $\Gamma$  is given as

$$\Gamma_m(E) = \nu [\Sigma^r(m; E) - \Sigma^{r\dagger}(m; E)] \quad (6)$$

and we denote

$$\mathcal{G}_l(E) = \mathcal{G}_{\bar{0}\bar{0}}(E + \frac{\hbar\omega l}{2}). \quad (7)$$

Now, we move on to the time-domain picture. Here, we will write the various Green's functions in time domain, viz.,

$$\mathfrak{G}_{nm}^r(t, t') = -\frac{i}{\hbar} \theta(t - t') \langle \{c_n(t), c_m^\dagger(t')\} \rangle, \quad (8)$$

$$\mathfrak{G}_{nm}^<(t, t') = \frac{i}{\hbar} \langle c_n^\dagger(t) c_m(t') \rangle \quad (9)$$

being the retarded and the lesser Green's functions respectively. Now we let our hamiltonian be time dependent, and split it into two parts,

$$\mathbf{H} = \mathcal{H} + \mathcal{V}(t) \quad (10)$$

Now, if we let  $\mathfrak{g}^r$  and  $\mathfrak{g}^<$  be the unperturbed Green's functions, then the full GFs are given via the Dyson equations as follows,

$$\mathfrak{G}^r = \mathfrak{g}^r + \mathfrak{g}^r * \mathcal{V} * \mathfrak{G}^r \quad (11)$$

$$\mathfrak{G}^< = \mathfrak{g}^< + \mathfrak{g}^r * \mathcal{V} * \mathfrak{G}^< + \mathfrak{g}^< * \mathcal{V} * \mathfrak{G}^r \quad (12)$$

where the symbol  $*$  stands for convolution w.r.t. time and matrix product w.r.t site indices. If we now integrate out the electrodes, we get,

$$G^r = g^r + g^r * (\Sigma^r + V) * G^r \quad (13)$$

and  $G^< = g^< + g^r * V * G^< + g^r * \Sigma^r * G^< + g^r * \Sigma^< * G^a + g^< * V * G^a + g^< * \Sigma^a * G^a$ . where the self-energies are defined in a similar manner, and the in-scattering matrices are related by the fluctuation-dissipation theorem as  $\Sigma^<(m; E) = \nu f_m(E) \Gamma_m(E)$ . With this in-hand, the expression for the current is given as a time derivative of the number density  $I_m = -e \langle d/dt \langle \hat{N}_m \rangle \rangle$  which is in turn defined as,

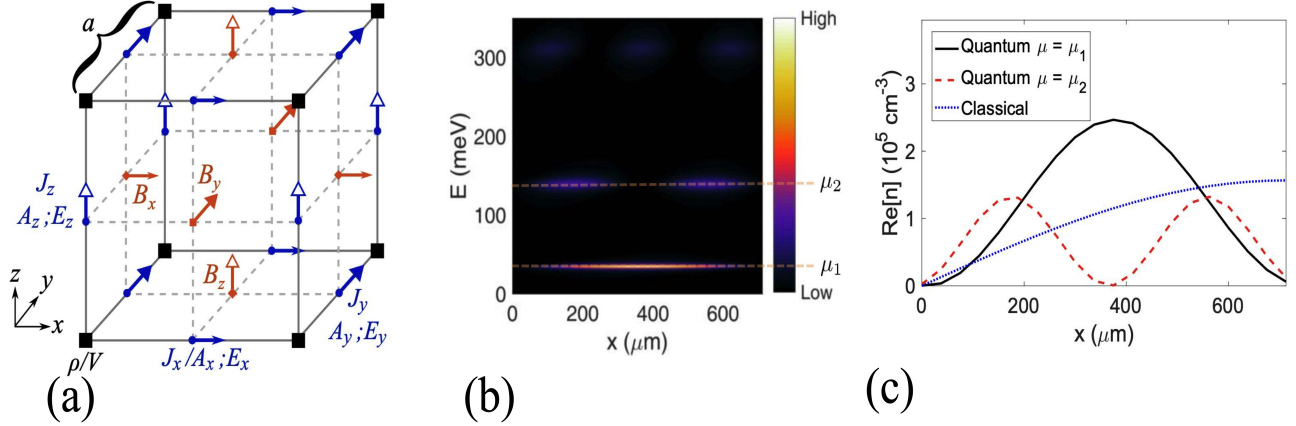


FIG. 2. (a) Yee cell for solving FDFD equations with side length  $a$ . The tight-binding Hamiltonian lattice where the charge density  $\rho$  is located by the solid squares at the corners of the grid. The potential  $V$  is naturally defined at the same positions. The current density,  $J_\alpha$ ,  $\alpha \in \{x, y, z\}$  is located between lattice sites, and hence the same component of the vector potential  $A_\alpha$  is also at these positions (b) Calculated LDOS (local density of states) plot of the quantum wire antenna, revealing the quantized states at  $\mu_1 = 34\text{meV}$  and  $\mu_2 = 140\text{meV}$ , which alter the macroscopic radiation pattern (c) Charge density distribution along the length of the antenna of the classical and the quantum cases. Figure(s) adapted from [16]

applied to the leads, the simplified expressions read,

$$\hat{N}_m = \sum_{\alpha \in \sigma_m} c_\alpha^\dagger(t) c_\alpha(t) \quad (14)$$

We get,

$$I_m(t) = e \sum_{i \in \sigma_0, \alpha \in \sigma_m} (\mathcal{V}_{\alpha i}(t) \mathfrak{G}_{i\alpha}^<(t, t) - \mathcal{V}_{i\alpha}(t) \mathfrak{G}_{\alpha i}^<(t, t)) \quad (15)$$

With this set of basics developed, the authors of [15] consider two type of AC perturbations (except screening),

1. *External AC Perturbation:* Uniform across the lead lattice points:

$$\mathbf{W} = eV_{ac}\mathbf{I}_{\bar{m}}$$

2. *Arbitrary internal AC perturbation:* Arbitrary matrix, single oscillating function, given as,

$$\mathbf{W} = eV_{ac}\mathbf{W}_{\bar{0}\bar{0}}$$

The paper goes further to give expressions for current and electronic density for these cases in the wide-band limit (WBL): wherein the contact self-energies are constant over the energy ranges considered. One simple application is applying an AC voltage across the gate of quantum point contact (QPC), the results of which are shown in Fig. 1.

## B. AC-NEGF with full electrodynamic coupling

The work in [16] reviews AC-NEGF equations first order in the perturbation in a simple and easy-to-implement manner. For the AC bias  $V(t) = V_{AC} \cos \omega t$

To first order, we have,

$$\sigma_\omega^r(E) = \frac{eV_{AC}}{\hbar\omega} [\Sigma_0^r(E) - \Sigma_0^r(E_+)] \quad (17)$$

$$g_\omega^r = G_0^r(E_+) [U_\omega + \sigma_\omega^r(E)] G_0^r(E) \quad (18)$$

where  $E_+ = E + \hbar\omega$  and  $U_\omega$  is the potential profile due to the AC voltage. Further, to first order the lesser GF correction is given as,  $g_\omega^<(E) = G_0^r(E_+) \Sigma_0^<(E_+) g_\omega^r(E)^\dagger + G_0^r(E_+) \sigma_\omega^<(E) G_0^r(E)^\dagger + g_\omega^r \Sigma_0^<(E) G_0^r(E)^\dagger$ .

Further, they note that these equations are inefficient as they require multiple inversions and integrations. To remedy this, they develop a recursive AC algorithm building on top of the DC algorithm. More notably, they develop a method to integrate the full solution of Maxwell's equations with the tight-binding NEGF by resorting to a Yee cell discretization which accounts for the lattice sites as well as the full electrodynamic potentials, as shown in Fig. 2 (a). Then a self-consistent procedure is employed to solve for the Green's functions and the potentials simultaneously. Finally, they apply this method to a quantum wire monopole antenna, whose LDOS plot is shown in Fig. 2 (b). Due to the quantization in the quantum case, the charge densities do not agree with the classical case, as can be seen in Fig. 2 (c). This leads to a different radiation pattern, and lesser directivity as a consequence.

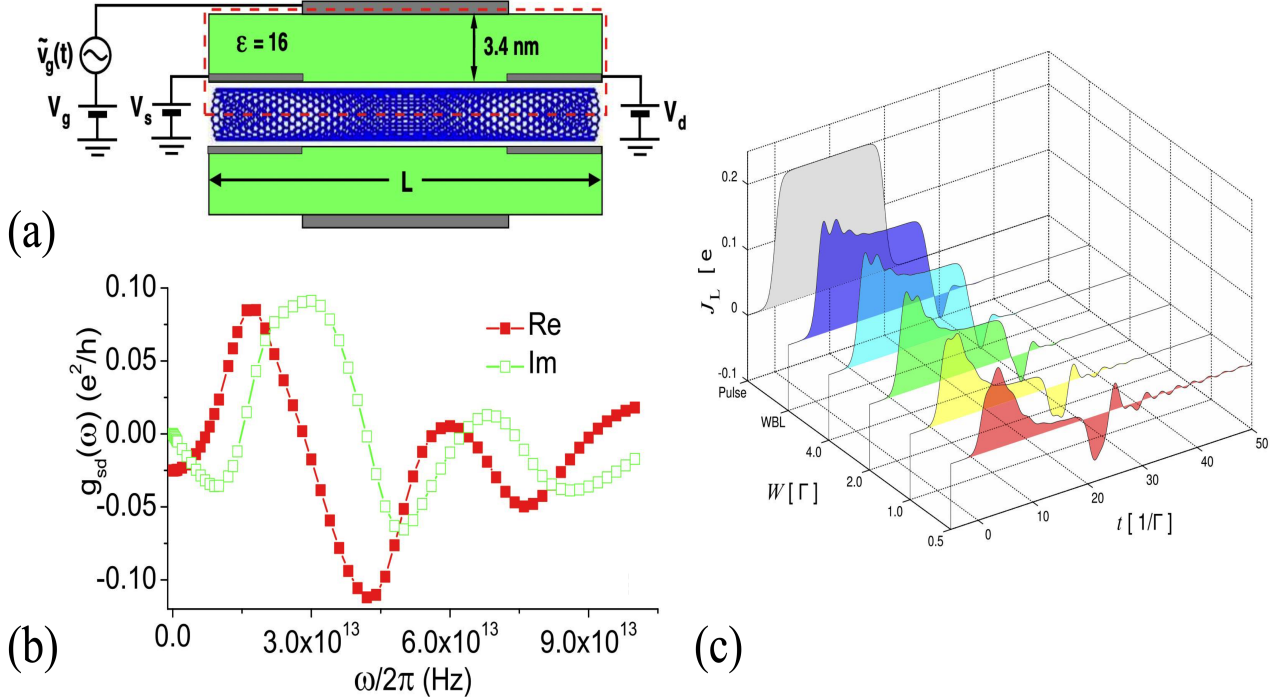


FIG. 3. (a) Schematic of the NTFET device considered in cylindrical geometry, embedded in a dielectric medium. The dashed rectangle specifies the computational domain. (b) AC response for the  $L = 20\text{nm}$  NTFET in the off state: real/imaginary part of the frequency- dependent conductance (c) Time-resolved current through left barrier, for different values of  $W$ , driven by a bias voltage pulse. The WBL corresponds to  $W \rightarrow \infty$ .

### C. Other attempts at AC-NEGF

Now that we have developed the basics and discussed primary attempts at AC-NEGF, we wrap up this section by briefly discussing some more attempts with interesting applications.

Kienle et al., in [18] use the Dyson equation approach coupled with a self-consistent evaluation of the potentials and densities to evaluate the high-frequency characteristics of a nanotube transistor (NTFET), which is schematically shown in Fig. 3 (a). The self-consistency arises with the following two equations,

$$\nabla[\epsilon(\mathbf{r})\nabla U(\mathbf{r}, E - E')] = -\rho(\mathbf{r}, E - E') \quad (19)$$

$$\rho(\omega) = \nu e \int \frac{dE}{2\pi} G^<(E_+, E) \quad (20)$$

wherein the first equation is simply the Poisson's equation, and the second is the equation for the frequency-dependent charge density. The resulting AC characteristics are shown in Fig. 3 (b).

In [19], Croy et al. obtain a viable propagation scheme at finite temperature using the Green's function approach via an auxilliary mode expansion. They assume the tunnel coupling functions to be factorized in energy and time, which enables using the expansion of the Fermi function as a sum over certain number of poles in the

equations of motion for the Green's functions. They solve the numerical problem in the WBL regime as well as using a Lorentzian ansatz. The approach is illustrated via a double quantum dot (DQD): the device consists of two QDs which are coupled in series. Each dot is also coupled to an electron reservoir. Owing two the series coupling, the broadening matrices have the form,

$$\boldsymbol{\Gamma}_L = \frac{1}{2} \begin{pmatrix} \Gamma(E) & 0 \\ 0 & 0 \end{pmatrix}; \quad \boldsymbol{\Gamma}_R = \frac{1}{2} \begin{pmatrix} 0 & 0 \\ 0 & \Gamma(E) \end{pmatrix} \quad (21)$$

The  $\Gamma(E)$  is either taken to be constant (WBL regime), or a Lorentzian  $\Gamma(E) = \Gamma_0 \times W^2 / (\varepsilon^2 + W^2)$ . A rectangular bias voltage,

$$V(t) = \frac{V_m}{2} \left( \tanh \frac{t}{t_s} - \tanh \frac{t - t_p}{t_s} \right) \quad (22)$$

The result is shown in Fig. 3 (c). The current shows a transient behavior at the beginning and after the end of the pulse. For sufficiently long pulses it settles to a new stationary value according to the plateau bias voltage  $V = V_m$ .

This ends the NEGF discussion. Now we move on to the scattering matrix approach. Before that, it is worth noting that there have been attempts at AC quantum transport in a tight-binding setting using quantum master approaches as well. For instance, see [20], where a

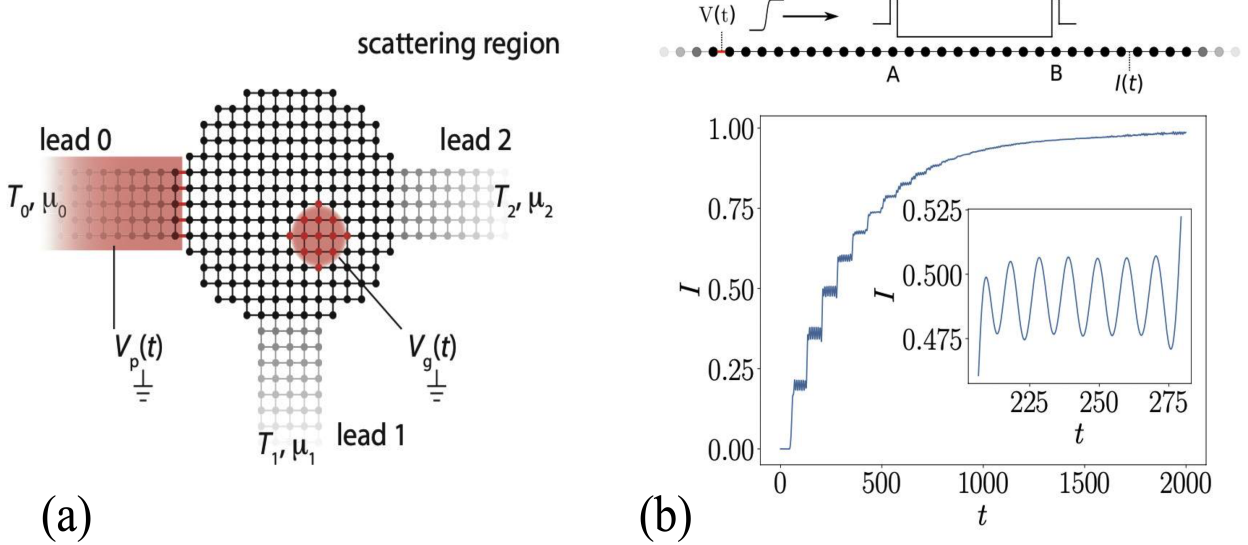


FIG. 4. (a) A typical system tackled by TKWANT. A central scattering region is connected to several leads. Each lead is a translationally invariant, semi-infinite system in thermal equilibrium. Sites and hopping matrix elements are represented by dots and lines. The regions in red indicate the time-dependent perturbation: in this example a global voltage pulse  $V_p(t)$  on lead 0 and a time-dependent voltage  $V_g(t)$  on a gate inside the scattering region (b) Fabry-Perot system: top panel shows a schematic of the system, a one-dimensional chain with potential barriers on sites A and B that transform the system into a Fabry-Perot cavity. Voltage pulse at left lead turns into a phase factor of the tunneling coefficient. Lower panel shows result of the simulation, current  $I(t)$  measured on the right of the two barriers A and B.

linear differential equation for an equal time two point correlator is derived using a Redfield quantum master equation under the Born-Markov approximation; current etc. observables are calculated.

### III. SCATTERING MATRIX APPROACHES

We outline the theoretical approach behind the algorithms of TKWANT [14]. Again, the setting is a tight binding hamiltonian

$$\hat{\mathbf{H}}(t) = \hat{\mathbf{H}}^s(t) + \sum_l \hat{\mathbf{H}}^l + \sum_{sl} \hat{\mathbf{H}}^{sl}(t) \quad (23)$$

where the first term is the scattering region (s), the second term is that of the leads (l) and the third is the coupling between the scattering region and the leads. This schematic is shown in Fig. 4 (a). Now, an important point is that any time dependence will be considered in only two ways:

- **Uniform** (global) potential across leads, which is identical across all the lead sites. A simple gauge transformation to the coupling hamiltonian  $\mathbf{H}_{in}^{sl}(t) \rightarrow e^{-i\phi^l(t)} \mathbf{H}_{in}^{sl}(t)$  accounts for this, with

$$\phi^l(t) = \frac{e}{\hbar} \int_{-\infty}^t V^l(\tau) d\tau \quad (24)$$

- Any arbitrary potential across the finite scattering region.

The general problem now addressed is the time evolution of observables such as densities or currents after the system is subjected to a time-dependent perturbation for  $t > t_0 (= 0)$ .

We have previously seen how ‘necessary’ quantities can be obtained using the NEGF approach. Let us now see how we can bypass that (sometimes excessively computational) method, and go back to it through a different manner. For  $t > t_0$  we write the hamiltonian as,

$$\hat{\mathbf{H}} = \hat{\mathbf{H}}_0 + \hat{\mathbf{W}}(t) \quad (25)$$

The stationary Schrödinger equation is  $\hat{\mathbf{H}}_0 \psi_\alpha = E_\alpha \psi_\alpha$ , from which the many body state for  $t < t_0$  can be written as

$$|\hat{\psi}\rangle = \prod_{E_\alpha < E_F} \hat{d}_\alpha^\dagger |0\rangle \quad (26)$$

with  $E_F$  as the Fermi level and,

$$\hat{d}_\alpha^\dagger = \sum_i \psi_\alpha^*(i) \hat{c}_i^\dagger \quad (27)$$

The scattering wavefunction formalism generalizes this to the case of infinite systems that consist of a finite scattering region connected to several leads in equilibrium.

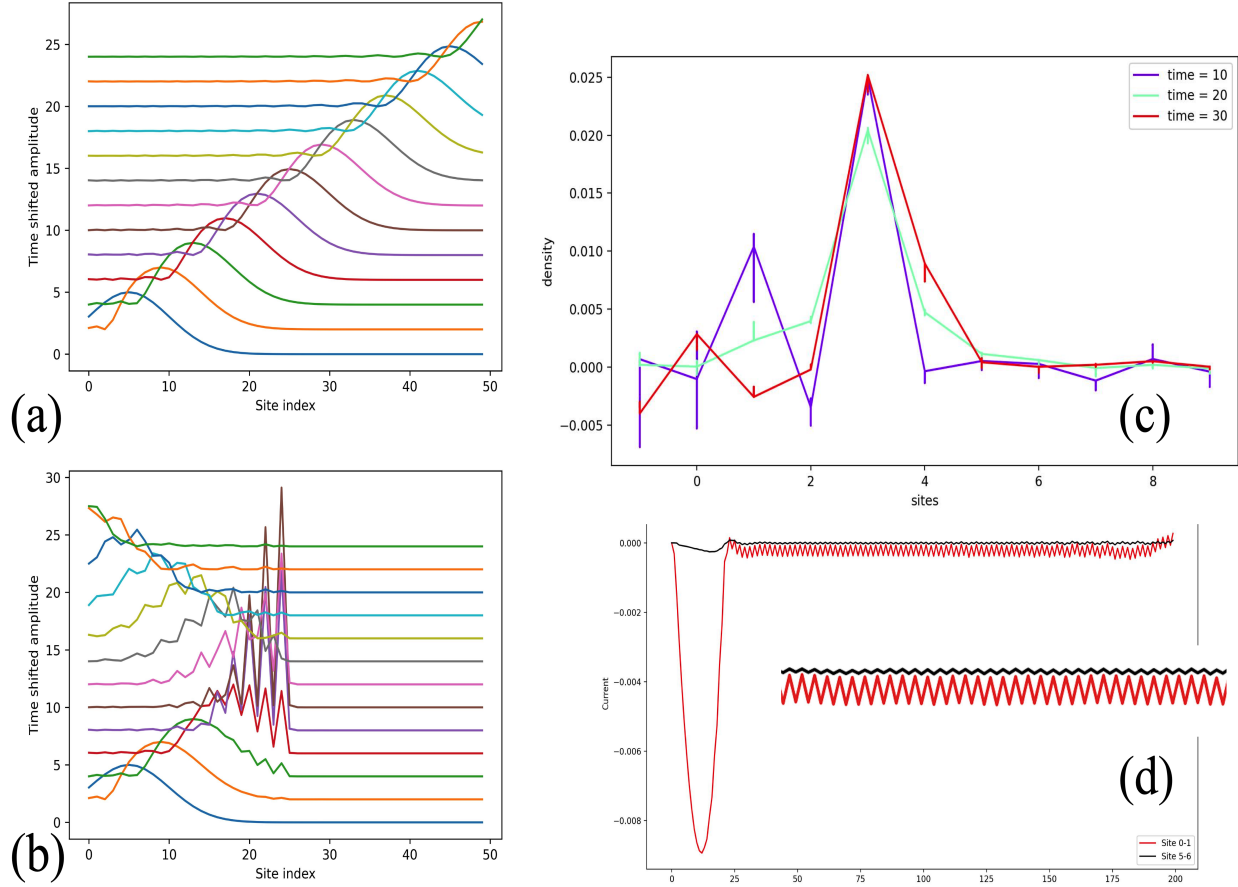


FIG. 5. (a) Propagation of a Gaussian wave packet across an infinite one-dimensional tight binding chain, simulated using TKWANT. (b) Simulating the same initial condition with a potential barrier in the middle of the wire, thus a reflection of the wave packet is observed (c) Density plots (density v. site) at different times when a normal-superconducting junction is probed with a square pulse at the normal lead (d) Hopping current as a function time between sites 0-1 (red) and sites 5-6 (black) when a spinless SSH chain is probed by a voltage of the form of Eq. 36

The theory is exact for arbitrary time-dependent perturbations. We partition the Hamiltonian as

$$\hat{\mathbf{H}} = \hat{\mathbf{H}}_0 + \hat{\mathbf{W}}(t) \quad (28)$$

The scattering wave functions  $\psi_{\alpha E}$  at  $t < t_0$  are now labeled by the energy, a continuous variable  $E$ , and a discrete index  $\alpha$  that labels all the conducting channels at energy  $E$  such that

$$\mathbf{H}_0 \psi_{\alpha E} = E \psi_{\alpha E} \quad (29)$$

The  $\psi_{\alpha E}$  are obtained from wave function matching between the incoming and outgoing modes in the leads. For  $t > t_0$ , we have,

$$i\partial_t \psi_{\alpha E}(t, i) = \sum_j \mathbf{H}_{ij}(t) \psi_{\alpha E}(t, j) \quad (30)$$

$$\psi_{\alpha E}(t < t_0, i) = \psi_{\alpha E}(i) e^{-iEt}$$

Some observable  $\mathbf{A}$  would then be calculated as,

$$\langle \hat{\mathbf{A}} \rangle(t) = \sum_{\alpha ij} \int \frac{dE}{2\pi} f_\alpha(E) \psi_{\alpha E}^*(t, i) \mathbf{A}_{ij} \psi_{\alpha E}(t, j) \quad (31)$$

In particular, the number  $n_i(t)$  of electrons on site  $i$  is

$$n_i(t) \equiv \langle \hat{c}_i^\dagger \hat{c}_i \rangle(t) = \sum_\alpha \int \frac{dE}{2\pi} f_\alpha(E) |\psi_{\alpha E}(t, i)|^2, \quad (32)$$

while the particle current  $I_{ij}(t)$  from site  $i$  to site  $j$  is

$$I_{ij}(t) = -2 \text{Im} \sum_\alpha \int \frac{dE}{2\pi} f_\alpha(E) \psi_{\alpha E}^*(t, i) \mathbf{H}_{ij} \psi_{\alpha E}(t, j), \quad (33)$$

It is good to note that the Green's functions can be computed from the scattering wavefunction easily (and the reverse is also possible),

$$\mathbf{G}_{ij}^R(t, t') = -i\theta(t - t') \sum_\alpha \int \frac{dE}{2\pi} \psi_{\alpha E}(t, i) \psi_{\alpha E}^*(t', j), \quad (34)$$

$$\mathbf{G}_{ij}^<(t, t') = i \sum_\alpha \int \frac{dE}{2\pi} f_\alpha(E) \psi_{\alpha E}(t, i) \psi_{\alpha E}^*(t', j). \quad (35)$$

A simple example where this approach can be illustrated is the Fabry-Perot interferometer. This is a simple model

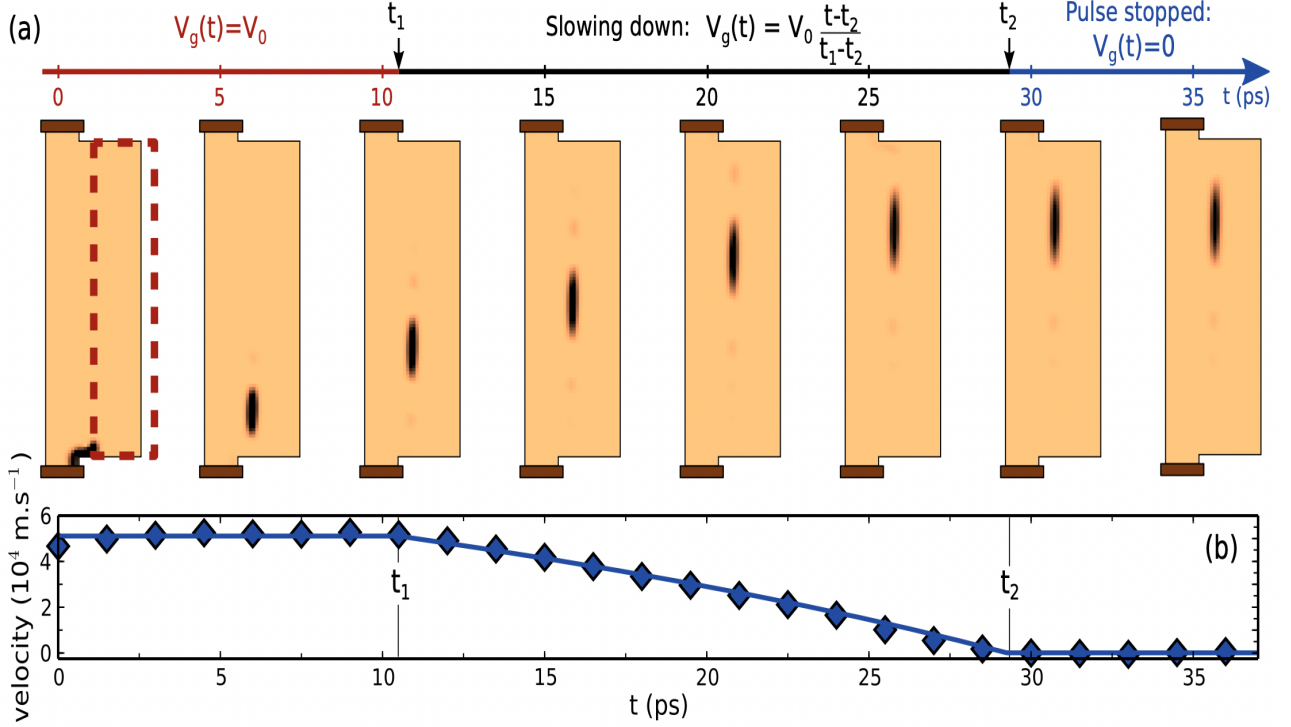


FIG. 6. (a) Charge density plotted at various times during the stopping protocol. The gate is polarized for  $t < t_1$  (thereby causing the edge mode at the center), and slowly grounded between  $t_1$  and  $t_2$ . At  $t = t_2$ , the pulse is stopped. (b) Velocity  $v(t)$  of the pulse as a function of time. Diamonds correspond to numerical data, the full line to the analytical result. Figure from [17]

of a device which can show a AC-Josephson-like phenomenon without superconductivity [21]. An infinite 1D chain has two potential barriers, as shown in Fig. 4 (b). A voltage pulse is applied at one lead,

$$V(t) = \begin{cases} 0, & \text{for } t < 0 \\ \frac{V_b}{2} \left(1 - \cos\left(\frac{\pi t}{\tau}\right)\right), & \text{for } 0 \leq t \leq \tau \\ V_b, & \text{for } t > \tau \end{cases} \quad (36)$$

and current plateaus are observed (Fig. 4 (b)), which exhibit oscillations at  $eV_b/h$ . Thus, a voltage to frequency conversion is realized without any superconductivity in play.

#### IV. NUMERICAL RESULTS

In this section, we show how the formalisms of AC quantum transport can be used to simulate known systems and investigates unknown AC responses of exotic systems. We perform these simulations usint TKWANT.

##### A. Simple Numerical Attempts

We start by performing a simple propagation of a one-dimensional wave-packet across an infinite wire. The initial condition is set using the wave-function feature in TKWANT, and then a one-body evolution of the TDSE is performed. The result is plotted in Fig. 5 (a). As expected, the wave packet propagates throughout the wire without any attenuation. Now, we know that if the packet faces a potential barrier, reflection would occur. To simulate this, we add a barrier of height  $U = 10 \times t$  at the middle of the scattering region. We see clear reflection and no transmission due to the large height of the barrier, as seen in 5 (b).

Now, we investigate a normal-superconducting junction in one-dimension – a system quite hot in the condensed matter community for phenomenon such as Andreev reflection and hosting Majorana modes. We apply a square pulse across the normal lead, and see the system response. The electron density across different sites, for times = 10, 20, 30 is plotted in 5 (c).

Lastly, we apply the voltage used in 36 across a SSH chain when it is in the topological phase. The system response shows oscillation at a characteristic frequency with different magnitudes at different lattice points, as seen in 5 (d). Unlike the Fabry-Perot cavity, we do not

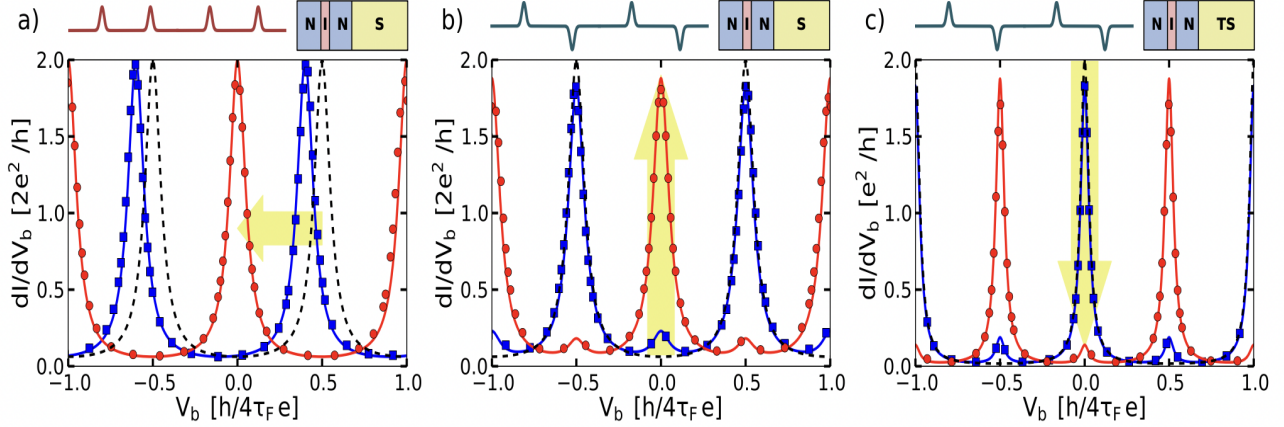


FIG. 7. DC conductance in the presence of a train of voltage pulses with small intensity  $\bar{n} = 0.1$  (blue squares) and large intensity  $\bar{n} = 0.5$  (red circles). Dashed line: no voltage pulse. Symbols: numerical simulations, lines: analytical model, Yellow arrows: evolution with increasing  $\bar{n}$ . The figure above each plot shows which type of voltage pulse train and system (regular S or topological superconductor TS) was used. Figure from [22]

see steps here as multiple paths are not possible owing to no barriers.

## B. Advanced simulation results

Here, we review the use of the AC quantum transport formalisms thus developed for more non-trivial cases.

Gaury et al. ([17]) proposed a method to control electron density pulses in a two-dimensional quantum hall sample. The system is a two-dimensional electron gas (2DEG) capacitively coupled with a top gate. The upper electrode is grounded, and the lower one is used to send AC pulses. The underlying physics is that when the gate voltage is ON, the edge state propagates along the middle of the sample, and when it is off, the edge mode propagates along the edge. This is a simple consequence of solving for the Landau levels. Now, the gate voltage is ON at  $t = 0$ . When a voltage pulse is sent at  $t = 0$ , the excitation starts propagation. Between  $t = t_1$  and  $t = t_2$ , the gate is slowly turned OFF. One thus finds that the excitation is stuck in its place for  $t > t_2$ . This can be seen in Fig. 6.

In [22], the interplay of Andreev and Majorana states at the interface of a normal-superconducting wire under the effect of a microwave AC drive is studied. It is found that the extra dynamical phase coming from the pulses can shift the phase of the Andreev reflection, resulting in the appearance of dynamical Andreev states. The results are shown in Fig. 7. For  $\bar{n} = 1/2$  one transforms the spectrum of a conventional superconductor into the

spectrum of a TS and vice versa. Also, for  $\bar{n} = 1/2$ , the train of pulses is equivalent to a train of alternating pulses. We see that upon increasing  $\bar{n}$  (using the amplitude of the pulses), a zero-bias peak develops while the Andreev peaks that were initially present shrink. Fig. 7(c) shows the effect of a similar alternating train on a system in the topological phase. We see that the initial zero-bias (Majorana) peak is effectively destroyed when  $\bar{n} = 1/2$  while new Andreev peaks appear; the dual to the previous situation. Anticipating what follows, they find that a simple monochromatic sine pulse  $\sim \cos \omega t$  (which can be seen as a distortion of the alternating pulse train) will have a similar, although slightly less marked, effect.

## V. CONCLUSIONS

In this paper, we have reviewed the NEGF and the scattering matrix formalisms for time-dependent quantum transport. We note that, while the Green's function approach allows for a systematic solving of various quantities, it is computationally expensive, as it involves multiple (large) matrix inversions and integrals. The scattering matrix, as shown by the development of KWANT and TKWANT has shown to be an approach which can be implemented numerically for large systems. Future work would include better algorithms such as the AC Recursive Green's Function (RGF) proposed in [16], simplifications of the Green's function approach which would further facilitate investigations of dephasing and disorder in the AC case as well.

[1] S. Reich, J. Maultzsch, C. Thomsen, and P. Ordejón, Tight-binding description of graphene, Physical Review

B **66**, 035412 (2002), publisher: American Physical Society.

- [2] A. H. C. Neto, F. Guinea, N. M. R. Peres, K. S. Novoselov, and A. K. Geim, The electronic properties of graphene, *Reviews of Modern Physics* **81**, 109 (2009), arXiv:0709.1163 [cond-mat].
- [3] G. Cohen, O. Hod, and E. Rabani, Constructing spin interference devices from nanometric rings, *Physical Review B* **76**, 235120 (2007), publisher: American Physical Society.
- [4] I. Žutić, J. Fabian, and S. Das Sarma, Spintronics: Fundamentals and applications, *Reviews of Modern Physics* **76**, 323 (2004), publisher: American Physical Society.
- [5] C. L. Kane and E. J. Mele, Quantum Spin Hall Effect in Graphene, *Physical Review Letters* **95**, 226801 (2005), publisher: American Physical Society.
- [6] C. L. Kane and E. J. Mele, Topological Order and the Quantum Spin Hall Effect, *Physical Review Letters* **95**, 146802 (2005), publisher: American Physical Society.
- [7] R. Shankar, Topological Insulators – A review (2018), arXiv:1804.06471 [cond-mat].
- [8] L. Arrachea, Stationary transport in mesoscopic hybrid structures with contacts to superconducting and normal wires: A Green's function approach for multiterminal setups, *Physical Review B* **79**, 104513 (2009), publisher: American Physical Society.
- [9] J.-F. Feng and S.-J. Xiong, Tunneling resonances and Andreev reflection in transport of electrons through a ferromagnetic metal/quantum dot/superconductor system, *Physical Review B* **67**, 045316 (2003), publisher: American Physical Society.
- [10] Electronic Transport in Mesoscopic Systems.
- [11] M. Moskalets, *Scattering Matrix Approach to Non-Stationary Quantum Transport: Chapter 1* (2011) p. 278.
- [12] M. Büttiker, A. Prêtre, and H. Thomas, Dynamic conductance and the scattering matrix of small conductors, *Phys. Rev. Lett.* **70**, 4114 (1993).
- [13] C. W. Groth, M. Wimmer, A. R. Akhmerov, and X. Waintal, Kwant: a software package for quantum transport, *New Journal of Physics* **16**, 063065 (2014).
- [14] T. Kloss, J. Weston, B. Gaury, B. Rossignol, C. Groth, and X. Waintal, Tkwant: a software package for time-dependent quantum transport, *New Journal of Physics* **23**, 023025 (2021).
- [15] O. Shevtsov and X. Waintal, Numerical toolkit for electronic quantum transport at finite frequency, *Physical Review B* **87**, 10.1103/physrevb.87.085304 (2013).
- [16] T. M. Philip and M. J. Gilbert, Theory of AC quantum transport with fully electrodynamic coupling, *Journal of Computational Electronics* **17**, 934 (2018).
- [17] B. Gaury, J. Weston, and X. Waintal, Stopping electrons with radio-frequency pulses in the quantum hall regime, *Physical Review B* **90**, 10.1103/physrevb.90.161305 (2014).
- [18] D. Kienle, M. Vaidyanathan, and F. Léonard, Self-consistent ac quantum transport using nonequilibrium green functions, *Physical Review B* **81**, 10.1103/physrevb.81.115455 (2010).
- [19] A. Croy and U. Saalmann, Propagation scheme for nonequilibrium dynamics of electron transport in nanoscale devices, *Physical Review B* **80**, 10.1103/physrevb.80.245311 (2009).
- [20] A. Purkayastha and Y. Dubi, Quantum transport under ac drive from the leads: A redfield quantum master equation approach, *Phys. Rev. B* **96**, 085425 (2017).
- [21] B. Gaury, J. Weston, and X. Waintal, The a.c. josephson effect without superconductivity, *Nature Communications* **6**, 10.1038/ncomms7524 (2015).
- [22] J. Weston, B. Gaury, and X. Waintal, Manipulating andreev and majorana bound states with microwaves, *Physical Review B* **92**, 10.1103/physrevb.92.020513 (2015).
- [23] N. S. Wingreen, A.-P. Jauho, and Y. Meir, Time-dependent transport through a mesoscopic structure, *Physical Review B* **48**, 8487 (1993).
- [24] X. Oriols and D. Ferry, Quantum transport beyond dc, *Journal of Computational Electronics* **12** (2013).
- [25] B. Hiltscher, M. Governale, and J. König, ac josephson transport through interacting quantum dots, *Physical Review B* **86**, 10.1103/physrevb.86.235427 (2012).
- [26] M. Fruchart, P. Delplace, J. Weston, X. Waintal, and D. Carpentier, Probing (topological) floquet states through DC transport, *Physica E: Low-dimensional Systems and Nanostructures* **75**, 287 (2016).
- [27] A. B. Michelisen, T. L. Schmidt, and E. G. Idrisov, Current correlations of cooper-pair tunneling into a quantum hall system, *Physical Review B* **102**, 10.1103/physrevb.102.125402 (2020).
- [28] R. Hussein, S. Kohler, J. C. Bayer, T. Wagner, and R. J. Haug, Spectral properties of stochastic resonance in quantum transport, *Physical Review Letters* **125**, 10.1103/physrevlett.125.206801 (2020).
- [29] D. V. Averin, G. Wang, and A. S. Vasenko, Time-dependent andreev reflection, *Physical Review B* **102**, 10.1103/physrevb.102.144516 (2020).
- [30] L. M. Gächter, R. Garreis, J. D. Gerber, M. J. Ruckriegel, C. Tong, B. Kratochwil, F. K. de Vries, A. Kurzmann, K. Watanabe, T. Taniguchi, T. Ihn, K. Ensslin, and W. W. Huang, Single-shot spin readout in graphene quantum dots, *PRX Quantum* **3**, 10.1103/prxquantum.3.020343 (2022).
- [31] J. Siegl, J. Picó -Cortés, and M. Grifoni, Particle conserving approach to ac-dc driven interacting quantum dots with superconducting leads, *Physical Review B* **107**, 10.1103/physrevb.107.115405 (2023).
- [32] M. Hashisaka, N. Hiyama, T. Akiho, K. Muraki, and T. Fujisawa, Waveform measurement of charge- and spin-density wavepackets in a chiral tomonaga-luttinger liquid, *Nature Physics* **13**, 559 (2017).
- [33] L. Luo, M. Mootz, J. H. Kang, C. Huang, K. Eom, J. W. Lee, C. Vaswani, Y. G. Collantes, E. E. Hellstrom, I. E. Perakis, C. B. Eom, and J. Wang, Quantum coherence tomography of light-controlled superconductivity, *Nature Physics* 10.1038/s41567-022-01827-1 (2022).
- [34] B. Gaury, J. Weston, M. Santin, M. Houzet, C. Groth, and X. Waintal, Numerical simulations of time-resolved quantum electronics, *Physics Reports* **534**, 1 (2014).
- [35] H. Haug and A.-P. Jauho, Quantum kinetics in transport optics of semiconductors, *Quantum Kinetics in Transport and Optics of Semiconductors: , Solid-State Sciences*, Volume 123. ISBN 978-3-540-73561-8. Springer-Verlag Berlin Heidelberg, 2008 **123** (2008).
- [36] M. Büttiker, A. Prêtre, and H. Thomas, Admittance of small conductors, *Phys. Rev. Lett.* **71**, 465 (1993).
- [37] M. P. Anantram and S. Datta, Effect of phase breaking on the ac response of mesoscopic systems, *Phys. Rev. B* **51**, 7632 (1995).
- [38] M. Buttikker, Capacitance, admittance, and rectification properties of small conductors, *Journal of Physics: Condensed Matter* **5**, 9361 (1993).

- [39] H. M. Pastawski, Classical and quantum transport from generalized landauer-büttiker equations, *Phys. Rev. B* **44**, 6329 (1991).
- [40] C.-M. Ho and J. T. Chalker, Models for the integer quantum Hall effect: The network model, the Dirac equation, and a tight-binding Hamiltonian, *Physical Review B* **54**, 8708 (1996), publisher: American Physical Society.
- [41] M. Koshino, H. Aoki, K. Kuroki, S. Kagoshima, and T. Osada, Hofstadter Butterfly and Integer Quantum Hall Effect in Three Dimensions, *Physical Review Letters* **86**, 1062 (2001), publisher: American Physical Society.